J. Phys. B: At. Mol. Opt. Phys. **29** (1996) 307–321. Printed in the UK

Comprehensive analysis of the stopping power of antiprotons and negative muons in He and H_2 gas targets

G Schiwietz†, U Wille‡, R Díez Muiño§, P D Fainstein‖[+] and P L Grande¶

† Bereich F, Hahn-Meitner-Institut Berlin, Glienicker Strasse 100, D-14109 Berlin, Germany
‡ Bereich T, Hahn-Meitner-Institut Berlin, Glienicker Strasse 100, D-14109 Berlin, Germany
§ Departamento de Física de Materiales, Facultad de Química, UPV/EHU, Aptdo. 1072, E-20080 San Sebastián, Spain
‖ Laboratoire de Chimie Physique—Matière et Rayonnement, Université Pierre et Marie Curie, 11 rue Pierre et Marie Curie, F-75231 Paris Cédex 05, France
¶ Instituto de Física da Universidade Federal do Rio Grande do Sul, Avenida Bento Goncalves 9500, BR-91500 Porto Alegre, Brazil

Received 15 June 1995

Abstract. A comprehensive analysis of the stopping power of antiprotons and negative muons in He and H_2 gas targets for projectile velocities (equivalent antiproton energies) ranging from about 0.1 to 10 au (0.25 keV to 2.5 MeV) is performed. Recent experimental data are contrasted with theoretical results obtained from different approaches. The electronic stopping power is evaluated within the coupled-state atomic-orbital method and the distorted-wave Born approximation as well as, for low projectile velocities, within a generalized adiabatic-ionization model that takes into account collisional-broadening effects. The departure of the antiproton stopping power from the proton stopping power ('Barkas effect'), observed for intermediate projectile velocities, is discussed. The contribution to the stopping power arising from energy transfer to the translational degrees of freedom of the target system ('nuclear stopping') is evaluated. Our analysis results in a good understanding of the stopping mechanisms of negative heavy particles in gases, in particular in He. Discrepancies between theory and experiment in the H_2 case are attributed to effects of the molecular structure of the target.

1. Introduction

The stopping cross section ('stopping power') of negatively charged, heavy particles traversing gas targets has only recently become a subject of investigation. At the CERN LEAR facility, the mean range and mean moderation time of antiprotons ($\bar{p}$) in He and H_2 targets were measured for kinetic energies ranging from about 0.5 keV to 1.1 MeV [1, 2]. The total stopping power $S^{\bar{p}}$ was deduced by assuming a parametrized energy dependence of $S^{\bar{p}}$ and determining the parameter values from a 'best fit' to the measured range curves and moderation time curves. In experiments performed at the 'muon-bottle apparatus' at PSI, the time distribution $L(t)$ of the scintillation light emitted from excited target atoms during the slowing down of negative muons (μ^-) in He and H_2 targets was measured for kinetic energies ranging between about 0.05 keV and 0.5 MeV [3–5]. The stopping power S^{μ^-} was derived from an analysis that uses the information provided by $L(t)$ along with experimental $\bar{p}$ ionization cross sections as well as other experimental and theoretical information.

[+] On leave from Centro Atómico Bariloche and Instituto Balseiro, Av. E Bustillo 9500, RA-8400 Bariloche, Argentina.

0953-4075/96/020307+15$19.50

Clearly, the total $\bar{p}$ and μ^- stopping powers at given projectile velocity v ought to be virtually identical, $S^{\bar{p}}(v) = S^{\mu^-}(v)$ (except for deviations at small v due to the mass dependence of the nuclear-stopping contribution). The experimentally determined values for $S^{\bar{p}}(v)$ and $S^{\mu^-}(v)$, however, deviate by about 20%. We assume these discrepancies to reflect the experimental errors and the uncertainties of the analyses. In the following, general discussion, we disregard the deviations and refer, for the sake of simplicity, mainly to the $\bar{p}$ case. The μ^- data will, of course, be explicitly included in the detailed comparison of the experimental data with theory.

The experimental data for He and H_2 targets have certain features in common, which make them particularly attractive for a detailed theoretical analysis. A marked feature is that for velocities v comparable to the velocity v_e of the active electron in the initial target state, i.e. for v in the vicinity of the stopping power maximum, the ratio of the $\bar{p}$ stopping power to the corresponding stopping power of protons is considerably smaller than unity. A similar behaviour, commonly referred to as the Barkas effect [6], has been observed already in the stopping power in solid targets [7, 8] and was also found in total cross sections for single ionization by protons and antiprotons in gas targets [9, 10]. The Barkas effect reflects the polarization of the target electron cloud due to the attraction (repulsion) exerted on the cloud when the proton (antiproton) passes by at larger distances from the target nucleus. This polarization is responsible for a breakdown of the first Born approximation which scales with the projectile charge number Z as Z^2 and which correctly describes the confluence of antiproton and proton data in the limit $v \gg v_e$.

When v decreases in the range $v < v_e$, the ratio of antiproton to proton stopping power rises (for H_2) or even becomes larger than unity (for He). Again, such a behaviour is known from the ionization cross sections [9, 10]. Qualitatively, it may be ascribed to the 'binding effect', which reflects the assumption that at low v electronic transitions occur predominantly in close (small-impact-parameter) collisions. When a proton (antiproton) penetrates slowly into the target electron cloud, it produces an increase (decrease) in binding energy of the initial target state, and thus the cross section is lowered (raised). However, when discussing the observed discrepancies between the proton and antiproton *stopping powers* at low v, it may be insufficient to invoke merely the binding effect. For $v < v_e$, the cross section for electron capture by protons may acquire the same order of magnitude as that of the cross sections for ionization and excitation. Hence, a considerable fraction of the incoming protons can be converted into (neutral) H atoms. The energy loss of H atoms colliding with target atoms differs from the energy loss of protons. The observed proton stopping power is a mean value over contributions from collisions of protons and of H atoms. For antiprotons, the electron capture channel is closed.

In the range $v \ll v_e$, the experiments have provided some evidence for an increase of the antiproton stopping power with decreasing v. This behaviour appears to deserve particular attention since for very low v a sizeable contribution to the stopping power should arise from nuclear stopping [11]. The electronic stopping in the low-v limit is expected to reflect the near-adiabatic behaviour of the projectile–target collision system. In near-adiabatic collisions induced by protons (or other positively charged, heavy projectiles), excitation and ionization can be understood in terms of transitions between the electronic states of the transiently formed 'quasimolecular' collision complex (see for example [12]). In collisions involving negative heavy projectiles, the electrons move in the field of the transient 'quasidipole' formed by the heavy particles. The electronic states of the quasidipole experience a monotonic loss of binding energy when the distance between the heavy particles decreases, and even become unbound at certain non-zero, 'critical' distances if the 'united atom' formed by the heavy particles does not support bound negative-ion states. This feature led Fermi

and Teller [13] and Wightman [14] to assume that 'adiabatic ionization' is the principal mechanism contributing to the stopping power of negative heavy particles in the low-v limit.

In this paper, we perform a comprehensive, quantitative analysis of the stopping power of antiprotons and negative muons in He and H_2 gas targets. The aim of this analysis is to provide insights into the basic mechanisms that are responsible for the slowing-down of negative particles in gases. We confront the existing experimental data with theoretical results obtained from different approaches and present a systematic comparison with the stopping power for protons. Particularly, we employ results of elaborate coupled-state atomic-orbital calculations that cover the electronic stopping over a broad v-range. The range of intermediate and high v is analysed within the distorted-wave Born approximation. For discussing the low-v limit, we devise and apply a generalized adiabatic-ionization model in which collisional-broadening effects are taken into account. The contribution of nuclear stopping is also evaluated.

In the next section, we briefly summarize the ingredients of the different models and approximations that will be used in our theoretical analysis of the experimental data. In section 3, we analyse the stopping power of negative particles in a He target. The stopping of negative particles in H_2 is considered in section 4, while section 5 contains a summarizing discussion. Unless stated otherwise, we use atomic units.

2. Theory

We assume the total stopping power S of a heavy particle to be decomposed into an electronic part S_e and a nuclear part S_n. The electronic stopping power S_e is, in general, a mean value [15] over contributions S_e^α from the different charge states α (with equilibrium fraction f_α) which the projectile can acquire in the target medium:

$$S_e = \sum_\alpha f_\alpha S_e^\alpha \tag{1}$$

$$S_e^\alpha = \sum_f \Delta E_{if} \sigma_{if}^\alpha \,. \tag{2}$$

Here, σ_{if}^α is the cross section for an electronic transition from the initial target state labelled i into a final state labelled f, and ΔE_{if} is the associated energy transfer. The sum over f extends over all bound and continuum states of target and projectile. For incoming protons, the mean electronic stopping power S_e^p comprises contributions from protons (H^+), H atoms (H^0) and negative H ions (H^-). As the H^- contribution is known to be very small [16], we will neglect it in the present analysis and write

$$S_e^p = f_+ S_e^+ + f_0 S_e^0 \,. \tag{3}$$

No averaging over charge states is required, of course, in the stopping power $S_e^{\bar{p}}$ of incoming antiprotons.

A general, non-perturbative method for calculating the stopping power of ions traversing atomic targets has been developed recently [17]. It is based on a coupled-state atomic-orbital (AO) description of the individual atomic collisions taking place in the target medium. A distinctive feature of the AO method is that, within the space of basis functions chosen in the expansion of the (time-dependent) scattering wavefunction, the full projectile–target interaction is treated in infinitely high order. In previous applications of the AO method, the basis was composed of up to ≈200 (bound and continuum) target-centred functions [17, 18], plus a projectile-centred hydrogenic 1s function for the case of proton projectiles [19]. The proton results for a He target have compared favourably with the available experimental

data. In particular, they have allowed the uncovering of the dominating role of the capture channel at intermediate and low v and its importance for explaining the deviations of the data [21, 22] from the v-proportionality assumed in semiempirical stopping power formulae [23].

The AO results that we apply here are largely taken from [18–20]. New calculations with up to 350 basis states have been performed for the $\bar{p}$He system. Further, we have extended the v-range to values below 0.6 au, using an improved representation of the wavepackets describing zero-energy electrons. Thereby, we avoid convergence problems with the AO expansion, which we had encountered previously, in particular for the $\bar{p}$H system. Here, instead of scaling the non-diagonal matrix elements of the lowest continuum wavepackets, we have performed a numerical integration over high-lying Rydberg states ($n > 7$) and low-lying continuum states in order to determine the zero-energy wavepackets. In doing so, we have exploited the fact that the energy dependence of the Rydberg wavefunctions and the continuum wavefunctions (provided the latter functions are normalized on the energy scale) is only weak near the nucleus. Thus, the high-lying Rydberg states are as accurately described as the continuum states in our previous work (atomic states with $n \leqslant 7$ are treated explicitly). This results in an improved representation of the quasidipole behaviour of the total wavefunction at low v.

It is noted that we have performed, within the AO method, test calculations for low v, in which the recoil effect [24] has been taken into account. This effect is of kinematic origin and represents the contribution to target ionization due to the recoil of the target nucleus arising from its interaction with the projectile nucleus. When the target nucleus becomes accelerated, the target electrons experience inertial forces which may induce ionization. For our cases, no indication for a significant contribution from the recoil effect was found.

In the present analysis, we further employ theoretical results obtained within the distorted-wave (DW) approach of [25, 26]. Specifically, this approach adopts the continuum-distorted-wave–eikonal-initial-state (CDW–EIS) model [27] (in conjunction with a hydrogenic description of the target) to calculate cross sections for bare projectiles, while for the neutral charge state the cross sections are obtained from the first Born approximation [28–30]. In DW approximations of this kind, higher-order effects are embodied in the initial-state and final-state wavefunctions, while the *residual* projectile–target interaction is treated in first order. Therefore, these approximations are expected to be valid at intermediate and high v. For proton stopping in He, the DW results for v above the stopping power maximum were indeed found [26] to be in very good agreement with the AO results and with the experimental data. Good agreement persists even for v far below the maximum.

For analysing the stopping power of antiprotons in the low-v range, we evaluate the electronic stopping power within a simple model that generalizes the adiabatic-ionization (AI) model of Fermi and Teller [13] and Wightman [14]. Starting from adiabatic potential curves for the electronic states in the field of the quasidipole formed by the antiproton and the nucleus of the target atom, we take into account the effect of the finite collision time by introducing a 'collisional broadening' of the potential curves [31]. From simple estimates for the velocity and impact parameter dependence of this broadening, we obtain the velocity dependence of the critical interparticle distances at which the broadened levels merge in the continuum.

Figure 1 shows adiabatic potential curves for the states of the $\bar{p}$H and $\bar{p}$He systems that are relevant to the present discussion (effects of the molecular structure of the H_2 target will be discussed below). The lowest curve (1σ) of the $\bar{p}$H system emerges from the H(1s) state at infinite interparticle distance R. With decreasing R, the binding energy of the 1σ state decreases monotonically and becomes zero at the 'critical' distance $R_c = 0.639$ au [13, 14].

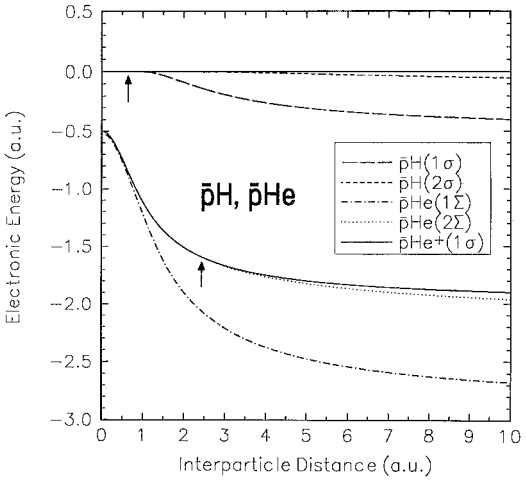

Figure 1. Adiabatic potential curves for electronic states of the $\bar{p}$H and $\bar{p}$He systems. The $\bar{p}$He(1Σ) and $\bar{p}$He(2Σ) curves are from [33], the other curves were calculated using the method of [32]. The upper arrow marks the critical distance at which the $\bar{p}$H(1σ) and $\bar{p}$H(2σ) curves merge in the continuum, the lower arrow the distance at which the $\bar{p}$He(2Σ) curve reaches the first ionization threshold.

The 2σ curve that originates from the H($n = 2$) manifold merges in the continuum at precisely the same R_c-value. It may be instructive to note that this property is shared by the infinity of σ-states which correspond to fixed spheroidal quantum number $n_\mu = 0$ (in the notation of [32]) and which are distinguished by different values of the spheroidal quantum number n_λ. While being independent of n_λ throughout, the critical distances R_c exhibit a monotonic increase with increasing angular momentum projection m and increasing n_μ [32]. All energy curves except the 1σ curve fall above the 2σ curve, so that no (real or avoided) curve crossings with the 1σ curve can occur.

The lowest curve (1Σ) of the $\bar{p}$He system [33] (see also [34, 35]) originates from the He($1s^2\ ^1S_0$) state at $R = \infty$ and rises monotonically, with decreasing R, towards the ground-state energy of the H^- ion at $R = 0$. The reference curve to which the 1Σ curve is to be compared in the present context is the 1σ curve of the $\bar{p}He^+$ system. This curve defines the lowest continuum threshold for the $\bar{p}$He system and hence the threshold for adiabatic ionization in this system. It is seen that the $\bar{p}$He(1Σ) curve stays consistently below the $\bar{p}He^+(1\sigma)$ curve. The $\bar{p}$He(2Σ) curve [33], on the other hand, reaches the threshold curve at $R_c = 2.4$ au. By analogy with the $\bar{p}$H case, we may assume that the 2Σ energy curve in the $\bar{p}$He system is a lower bound to any curve except the 1Σ curve and that crossings with the latter curve will not occur.

The behaviour of the potential curves shown in figure 1 suggests that, in a strictly adiabatic picture, the ionization probability in collisions of antiprotons with (ground-state) H atoms is unity if the distance of closest approach R_0 is below $R_c = 0.639$ au, and zero otherwise. As no crossings of the 1σ curve with other curves occur, the probability for excitation to bound H states will be zero throughout. For collisions of antiprotons with (ground-state) He atoms, zero probabilities are expected for both ionization and excitation. We suspect, however, that for antiproton interactions with atoms the strictly adiabatic picture may not be fully adequate even at very low v.

It is seen from figure 1 (see also figures 3 and 6 below) that the $\bar{\mathrm{p}}\mathrm{H}(1\sigma)$ energy curve varies only weakly with R when R rises from R_c to $\approx$1.5 au. Similarly, the $\bar{\mathrm{p}}\mathrm{He}(1\Sigma)$ curve stays close to the continuum threshold for R up to $\approx$1 au. In this situation, the critical distances $R_\mathrm{c}^{(v)}$ at which the *broadened* energy curves *start to overlap* with the continuum are expected to depend strongly on v. Such a behaviour differs from the case of 'level promotion into the continuum' in heavy (many-electron) quasimolecular collision systems [12, 36]. In that case, strongly promoted levels like, for example, the $4\mathrm{f}\sigma$ level, experience a rapid loss of binding energy in a narrow R-range, so that the critical distances and the ionization cross sections derived therefrom depend only weakly on v.

For calculating the electronic stopping power of antiprotons within our generalized adiabatic-ionization model, we write the collisional broadening $\Gamma^{(v)}(b)$ for a collision at velocity v and impact parameter b as

$$\Gamma^{(v)}(b) = 1/\tau^{(v)}(b) = v/a(b) \tag{4}$$

where $\tau^{(v)}(b)$ is a characteristic interaction time and $a(b)$ the associated characteristic length. Generalizing a prescription given by Bohr [37], we take

$$a = d + 2b \tag{5}$$

where d is the 'diameter' of the unperturbed target electron cloud. This expression for a appears to represent a plausible interpolation between the limiting cases of small and large impact parameters. Here, we use

$$d = 2r_\mathrm{K} \tag{6}$$

where r_K is the mean K-shell radius of the H or He atom. Hence,

$$\Gamma^{(v)}(b) = \frac{v}{2(r_\mathrm{K} + b)}\,. \tag{7}$$

In the present cases, b can be safely identified with the distance of closest approach R_0. Then, assuming the adiabatic energy curves to become symmetrically broadened, we can determine the critical distance $R_\mathrm{c}^{(v)}$ associated with a broadened curve from the condition

$$\left|E(R_\mathrm{c}^{(v)})\right| = \frac{\Gamma^{(v)}(R_\mathrm{c}^{(v)})}{2} \tag{8}$$

where $E(R)$ is the adiabatic energy as measured from the continuum threshold. Finally, the electronic stopping power (per atom) of antiprotons is calculated as

$$S_\mathrm{e}^{\bar{\mathrm{p}}}(v) = 2\pi \int_0^{R_\mathrm{c}^{(v)}} \mathrm{d}b\, b\overline{\Delta E_{\bar{\mathrm{p}}}} = \pi\,\overline{\Delta E_{\bar{\mathrm{p}}}}\left[R_\mathrm{c}^{(v)}\right]^2 \tag{9}$$

where $\overline{\Delta E_{\bar{\mathrm{p}}}}$ is the mean energy loss of the antiproton. Within the near-adiabatic picture, it is reasonable to identify $\overline{\Delta E_{\bar{\mathrm{p}}}}$ with the first ionization potential of the target system.

In evaluating the nuclear-stopping contribution $S_\mathrm{n}^{\bar{\mathrm{p}}}$ for antiproton energies equal to or larger than 1 keV, we use the prescription of [17]. For energies below 1 keV, we apply perturbation theory. This corresponds to the use of time-independent projectile–target interaction potentials, as they are assumed in most nuclear-stopping models [23, 37]. The perturbative results are normalized to the results of the full calculation at 1 keV (the value of the normalization factor is close to unity).

3. Stopping power of negative particles in He

Turning now to the detailed analysis of the stopping power of negative particles in gas targets, we begin by considering stopping in He targets. We have chosen to discuss the He case first because we found its analysis simpler than that of the H_2 case where specific difficulties seem to arise from the molecular structure of the target.

In figure 2, the CERN antiproton data [2] and the PSI negative-muon data [3, 4] for He are plotted against the projectile velocity v and against the 'equivalent' antiproton energy. Also shown are our theoretical results for the electronic stopping power as well as for the nuclear stopping power of antiprotons. When comparing theory and experiment, we assume, in conformity with the estimates given in [2], uncertainties of about $\pm 10\%$ in the $\bar{p}$He data. Uncertainties in the μ^-He data [3, 4] are about $\pm 10\%$ for v beyond, and in the vicinity of, the stopping-power maximum, and increase rapidly to more than $\pm 50\%$ with decreasing v. Therefore, a separate comparison with the $\bar{p}$ and μ^- data, respectively, does not make sense. Rather, it is appropriate to compare the theoretical results to an average stopping power curve that is defined as the (unweighted) mean value of $S^{\bar{p}}$ and S^{μ^-} down to $v \approx 1$ au, and that rapidly approaches the $\bar{p}$ stopping power for smaller v.

The maximum of the experimentally determined stopping power in figure 2 is located at a projectile velocity slightly larger than the mean velocity $v_K(\mathrm{He}) = 1.697$ au of the He K-shell electrons. Both the AO and the DW results reproduce the position and the height of the maximum as well as the high-v tail of the data within the experimental uncertainties. Deviations of the AO and DW results from the ordinary first-order Born approximation, which show up for v smaller than ≈ 4 au, indicate the onset of higher-order effects of the projectile–target interaction. Below the maximum, the AO and DW results progressively diverge with decreasing v. The AO results (including the nuclear-stopping contribution) stay consistently above the data, with deviations increasing from 15% at $v = 1$ au to 80% at $v = 0.2$ au.

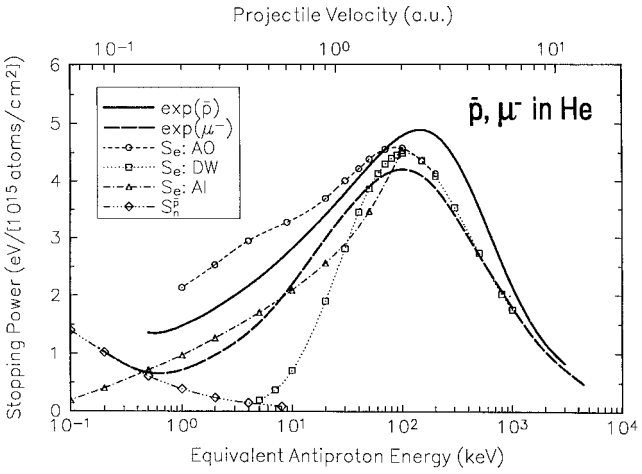

Figure 2. Stopping power (per atom) of antiprotons and negative muons in a He target, plotted as a function of projectile velocity v and of equivalent antiproton energy. The experimental results for $\bar{p}$ are from [2], those for μ^- from [3]. Our theoretical results for the electronic stopping power S_e have been obtained from the coupled-state atomic-orbital (AO) method, the distorted-wave (DW) approach, and the generalized adiabatic-ionization (AI) model, respectively. Also shown is our theoretical result for the nuclear stopping power S_n^p of antiprotons.

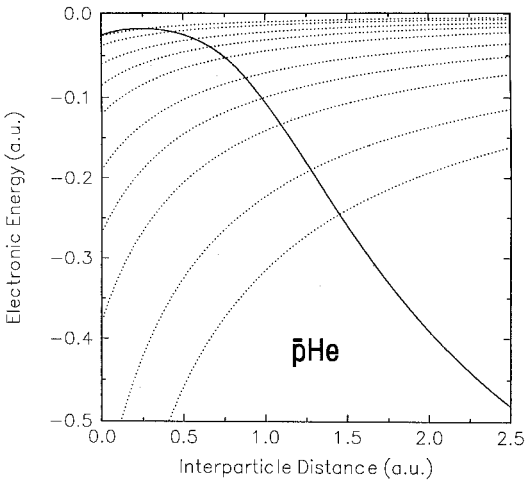

Figure 3. Full curve: the $\bar{p}He(1\Sigma)$ energy, referred to the continuum threshold as given by the $\bar{p}He^{+}(1\sigma)$ energy curve of figure 1. Dotted curves: the function $-\Gamma^{(v)}(R)/2$ (cf. equation (7)) with $r_K(He) = 0.5906$ au, plotted for projectile velocities v corresponding to equivalent antiproton energies of 0.1, 0.2, 0.5, 1, 2, 5, 10, 20, 50 and 100 keV (from top to bottom). The points of intersection of the dotted curves with the full curve define the critical distances $R_c^{(v)}$ (cf. equations (8) and (9)).

To understand the deviations between the AO results and the data, it is important to realize that our AO model treats *one* active electron moving in the potentials of the heavy particles and of the *fixed* (ground-state Hartree–Fock) density distribution associated with the second (inactive) electron. Within the frame of this model, the accuracy of our results is about 3%. Thus, any larger deviation from the data is to be attributed essentially to *dynamic* two-electron effects. The *overestimation* of the data by our results in the low-v (near-adiabatic) range can be ascribed to a lowering of the effective ionization threshold as compared with a fully relaxed two-electron treatment, which gives a threshold of $\approx$0.7 eV at $R = 0$ in the $\bar{p}He$ system (cf. figures 1 and 3). In fact, a sample calculation has shown that in the adiabatic limit of our one-electron AO model, no bound state exists at $R = 0$, i.e. there is no ionization threshold. Therefore, the present AO calculations are expected to overestimate the inelastic cross section, in particular the ionization cross section, and hence also the electronic stopping power. Indeed, the AO ionization cross section for $\bar{p}He$ collisions turns out to be significantly larger than the measured cross section [9] for antiproton energies below 40 keV.

In contrast to the $\bar{p}He$ case, *proton* stopping in He is not expected to be greatly affected by near-adiabatic two-electron effects. In the pHe system, the ionization potential at $R = 0$ is overestimated by 15% in our one-electron AO model. The resulting underestimation of the target ionization cross section is not crucial because the proton stopping power in the low-v range is dominated by the capture and loss channels. These channels are reasonably well described in the AO model [19] as well as in the DW approach [26].

The DW stopping power for antiprotons in He exhibits, below the stopping power maximum, a much steeper decrease than do the data. Total DW cross sections for single ionization in low-v $\bar{p}He$ collisions, on the other hand, are in very good agreement with the experimental data [9]. Hence, the deviation of the DW stopping power from the data is to be attributed to an underestimation of the calculated excitation cross section (note that measurements of excitation cross sections for $\bar{p}He$ collisions are not available). When comparing DW and AO results at low $\bar{p}$ velocities, one has to keep in mind that in the DW approach, in addition to the incomplete treatment of two-electron effects, higher orders of the residual projectile–target interaction are neglected. Therefore, a qualitatively different behaviour of AO and DW results is no surprise.

To obtain the AI results shown in figure 2, we have solved (8) for $R_c^{(v)}$ (cf. figure 3 for the graphical solution), identifying $E(R)$ with the difference of the $\bar{p}He(1\Sigma)$ and $\bar{p}He^{+}(1\sigma)$

energies of figure 1. The stopping power was calculated from (9), with $\overline{\Delta E_{\bar{p}}}$ taken equal to 24.58 eV, i.e. to the first ionization potential of the He atom. In the low-v range, the experimental data are to be compared to the sum of AI result and the calculated nuclear-stopping contribution. As the uncertainties of the low-v μ^- data are much larger than those of the $\bar{p}$ data, it is appropriate to add $S_n^{\bar{p}}$ to the AI stopping power and compare the sum curve (not shown in figure 2) to the average data curve defined above (i.e. essentially to the $\bar{p}$ data). The sum curve coincides with the data curve at the low-v end of the latter curve and, moreover, exhibits a minimum there, in agreement with the tendency observed in the data. For larger v, the sum curve stays below, but close to, the data curve, with the deviations not exceeding 20%. Assuming an average experimental uncertainty of $\pm 10\%$ (see above), we find that the calculated sum of AI and nuclear stopping powers is in quite good agreement with the data.

In view of the simplicity of our AI model, this appears to be a remarkable result, the more so as we have fixed the specific form and the parameter values of the input quantities (potential curves, collision broadening) *a priori*, i.e. no fitting to the data has been performed. Since the calculated AI stopping power is in general quite sensitive to changes in the input quantities, we believe that the good agreement between theory and experiment is a *non-trivial* result that reflects the correctness of our assumption that ionization out of the quasidipolar collision complex is the principal stopping mechanism for slow negative particles in gases. The theoretical description of near-adiabatic ionization in negative-particle collisions with atoms is, of course, a simpler task than in collisions of positive particles. In the former case, the near-adiabatic dynamics is governed essentially by the coupling of the electronic ground state of the quasidipole to a quasicontinuum of very loosely bound states and to the true continuum. So it appears somewhat plausible that this coupling can be adequately treated in terms of a simple collisional-broadening model. In positive-particle collisions, one has to deal, in general, with a large number of bound quasimolecular states as well as with the two-centre continuum [12]. No consistent treatment of positive-particle stopping within a quasimolecular approach, in particular for light collision systems, has been attempted yet.

We note that our AI model can be applied also to *single ionization* of atoms by negative-particle impact. The corresponding total cross section is immediately obtained from (9) by removing the mean energy loss $\overline{\Delta E_{\bar{p}}}$. For $\bar{p}$He collisions, the AI cross section turns out to be larger than the experimental ionization cross section [9] by a factor of two to three for $\bar{p}$ energies between 10 and 50 keV. Qualitatively, this discrepancy can be easily explained. The stopping power is largely determined by electronic transitions into highly excited bound states and low-lying continuum states. In the AI model, all these transitions are effectively taken into account by identifying the mean energy loss with the first ionization potential. The experimental ionization cross section, on the other hand, comprises only transitions into the true continuum. Therefore, in general, the AI ionization cross section is expected to overestimate the experimental cross section considerably. It is noted, however, that for $\bar{p}$He (and for any other collision system whose ground-state potential curve stays below the ionization threshold for all R) the AI model predicts vanishing ionization cross sections for very low v (cf. figure 3). The projectile energy below which the ionization cross section, and hence the AI stopping power, are predicted to vanish is slightly smaller than 0.1 keV for $\bar{p}$He collisions.

We now consider the *ratio* of antiproton to proton stopping power in He (note that no measurements of the stopping power of positive muons exist, so that an independent analysis based solely on muon data cannot be performed). In figure 4, this ratio is shown as a function of projectile velocity and projectile kinetic energy. The experimental data

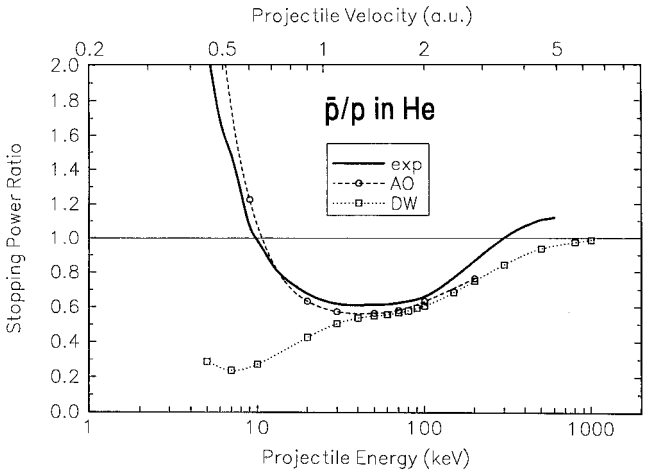

Figure 4. Ratio of antiproton to proton stopping power in He, plotted as a function of projectile velocity v and of projectile kinetic energy. The curve labelled 'exp' has been derived from the $\bar{p}$ data of [2] and from the proton data of [21] (3 to 20 keV) and [38] (40 to 600 keV). The AO stopping power for protons is taken from [19], the DW stopping power for protons from [26].

exhibit the Barkas effect, with a pronounced minimum with values as small as 0.6 for $v \approx 1.2$ au. Theoretical stopping power ratios have been obtained by combining the present AO and DW results for antiprotons with the corresponding proton results of [19, 26]. Down to the minimum, the theoretical ratios appear to agree with the data within the experimental uncertainties. The different behaviour of AO and DW ratios below the minimum reflects essentially the differences in the corresponding $\bar{p}$ stopping powers as exposed by figure 2. The AO method, while somewhat overestimating the stopping power ratio below $v \approx 0.6$ au, correctly predicts the rapid rise of the ratio below the minimum. The failure of the DW method to do so clearly indicates the importance of higher orders of the residual projectile–target interaction in the description of slow collisions of negative particles with atoms.

In concluding this section, we mention that the results of recent classical-trajectory Monte Carlo (CTMC) calculations [20] for the $\bar{p}$ stopping power in He are in good agreement with the present AO results, in particular for projectile energies below 100 keV.

4. Stopping power of negative particles in H_2

In figure 5, the experimental data for $\bar{p}$ and μ^- stopping in H_2 are shown along with our theoretical results. The stopping power (per atom) for H_2 is seen to bear a close resemblence to the He data of figure 2, except for an overall reduction by about 20%. The maximum of the H_2 data shows up at $v \approx 2$ au. This velocity is considerably larger than the Heitler–London estimate $v_{^1\Sigma_g} = 0.946$ au for the mean electron velocity in the $^1\Sigma_g$ ground state of the H_2 molecule.

The H_2 data are compared in figure 5 to AO and DW results obtained for *atomic* hydrogen. For v beyond the observed stopping power maximum, agreement between experiment and theory is found within the experimental uncertainties (the estimated uncertainties of the H_2 data are about the same as those of the He data; cf. section 3). This shows that in collisions with fast projectiles, the H_2 molecule essentially behaves as a collection of two independent H atoms. In fact, AO and DW ionization cross sections for $\bar{p}$ impact on *atomic* hydrogen are

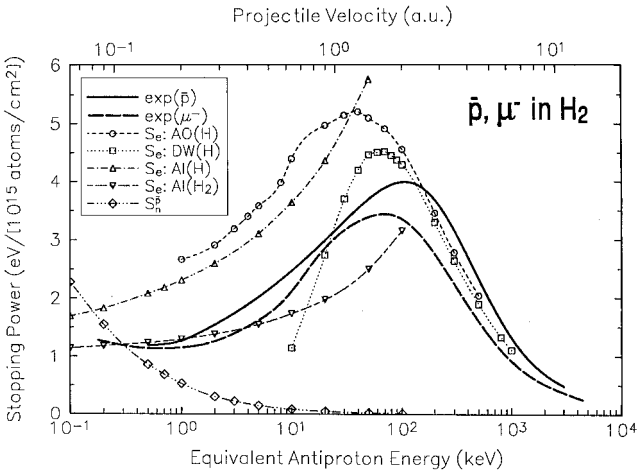

Figure 5. Stopping power (per atom) of antiprotons and negative muons in an H_2 target, plotted as a function of projectile velocity v and of equivalent antiproton energy. The experimental results for $\bar{p}$ are taken from [2], those for μ^- from [4]. Theoretical results are shown for electronic stopping in *atomic* hydrogen (AO, DW, AI) as well as in H_2 (AI). Also shown is our theoretical result for $S_n^{\bar{p}}$ corresponding to H_2.

both consistent with recent data [10] over the full energy range covered by the experiments ($\geqslant$30 keV). For v in the vicinity of, and below, the observed stopping power maximum, neither of the two theoretical approaches is able to provide a satisfactory explanation of the data. The deviations of the AO stopping power from the data are particularly striking. As the AO calculations for the (one-electron) H atom are estimated to be accurate within $\approx$3%, these deviations are to be attributed essentially to effects of the molecular structure of the H_2 target.

Also shown in figure 5 are AI results for atomic hydrogen (cf. figure 6). While grossly overestimating the data, the AI stopping power deviates from the AO stopping power by about 10% only. This agreement indicates the basic validity of the two theoretical approaches in the description of stopping in one-electron targets at low projectile velocities. It is noted that, to some extent, our AO results for atomic hydrogen may be used to optimize the form of the collisional broadening $\Gamma^{(v)}(b)$ in the AI model. Taking, for example, $a = 2r_K + b$ in (4), instead of the Bohr expression (5), we would obtain very good agreement between AO and AI results for atomic hydrogen below $v = 1$ au, and improved agreement between AI results and the He data. Here, however, we adhere to (5) throughout.

A complete evaluation of the dynamics of negative-particle stopping in molecular targets is beyond the scope of the present investigation, but molecular-structure effects can be included, admittedly in a crude way, in the AI model.

In general, the treatment of near-adiabatic collisions of atomic particles with diatomic molecules relies on electronic potential-energy hypersurfaces defined in the configuration space of the three heavy particles. In the present case, the projectile motion, while being slow with respect to the electronic motion in the target molecule, is still fast as compared with the internal motion of the heavy particles in the molecule. We can therefore assume that the interparticle distance in the molecule remains virtually unchanged during electronic transitions, i.e. that the Franck–Condon principle holds. We are then left with the problem of calculating the electronic energy as a function of the distance between projectile and centre of mass (or centre of charge) of the molecule and as a function of the angle between

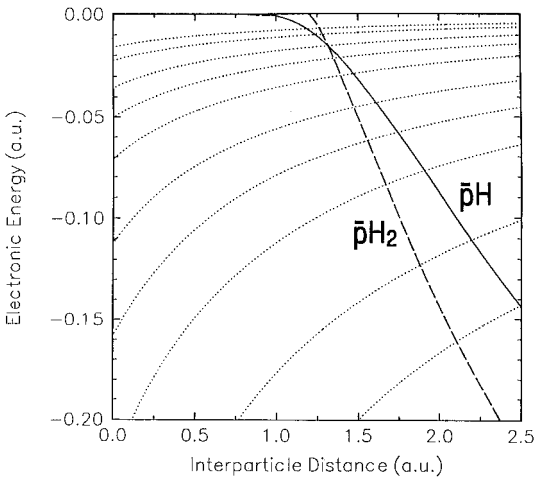

Figure 6. Full curve: the $\bar{p}H(1\sigma)$ energy curve (cf. figure 1). Long-broken curve: difference between the lowest effective energy curve of the $\bar{p}H_2^+$ system and the lowest curve of the $\bar{p}H_2$ system, obtained by describing the H_2^+ and H_2 molecules in the 'quasiatomic' approximation (see the text). Dotted curves: the function $-\Gamma^{(v)}(R)/2$ (cf. equation (7)) with $r_K(H) = 1.0$ au, plotted for the projectile velocities v of figure 3. For further explanation, see the caption to figure 3.

the symmetry axis of the molecule and an arbitrary space-fixed axis. As this problem is still too complicated to be solved with reasonable effort, we introduce a 'quasiatomic' description of the diatomic molecule, in which the effect of the two nuclear charges is replaced with that of a single (effective) charge Z^{eff} located at the centre of charge of the molecule. Adopting an independent-electron model, we choose Z^{eff} such that the total electronic energy of a given molecular state is reproduced. Effects of averaging over the spatial orientation of the molecule are not explicitly taken into account in the quasiatomic picture. We believe, however, that, to some extent, this averaging is implicitly allowed for by replacing the nonspherical electronic potential of the molecule with a spherical one. Within the quasiatomic description of the target molecule, our generalized adiabatic-ionization model can be directly applied by identifying the interparticle distance R with the distance between projectile and centre of charge of the molecule.

For H_2, we choose $Z^{\text{eff}}_{H_2} = 1.371$ in order to reproduce the total electronic energy of the molecule at its equilibrium internuclear distance of 1.402 au. As in the $\bar{p}He$ case, we assume threshold ionization to be the principal excitation mechanism also in the $\bar{p}H_2$ system. According to the Franck–Condon principle, the final electronic state to be considered is then the lowest H_2^+ state at an internuclear distance of 1.402 au. The electronic energy at this distance is reproduced by choosing $Z^{\text{eff}}_{H_2^+} = 1.603$. The effective $\bar{p}H_2^+$ and $\bar{p}H_2$ energy curves in the quasiatomic approximation are readily calculated by using the method of [32]. Their difference, shown in figure 6 in comparison with the $\bar{p}H$ curve, becomes zero at $R_c = 1.20$ au, i.e. the $\bar{p}H_2$ curve reaches the continuum threshold at this distance. The critical distances $R_c^{(v)}$ corresponding to the $\bar{p}H_2$ curve are calculated by taking $r_K = 1$ au, i.e. the mean K-shell radius of the H atom, in (7) for the collisional broadening. This choice is consistent with a rough estimate for the 'radius' of the (spatially averaged) H_2 ground-state density distribution [39]. Due to the steep decrease of the $\bar{p}H_2$ energy curve, the critical distances

are not very sensitive to changes in this radius anyhow.

Evaluating equation (9) with $\overline{\Delta E_{\bar{p}}}$ equal to 16.183 eV, i.e. to the first ionization potential of the H_2 molecule, we obtain the electronic stopping power *per target molecule*. The electronic stopping power *per target atom* shown in figure 5 is found to be considerably smaller than the AI result for the $\bar{p}$H system. However, upon adding the contribution of nuclear stopping, the theoretical results nevertheless overestimate the experimental data in the low-v range. With increasing v, the theoretical stopping power tends to become somewhat smaller than the data (note that inclusion of the double-ionization channel $H_2 \rightarrow 2H^+ + 2e^-$ would increase our AI results by about 10% at an equivalent antiproton energy of 50 keV). Nevertheless, on average, our crude method to include molecular-structure effects in the AI model appears to give improved agreement with the data.

Ratios of antiproton to proton stopping powers for H_2 are shown in figure 7. The experimental ratio is close to that for He (cf. figure 4) for $v > 1.0$ au, i.e. the Barkas effect is clearly visible also in the H_2 data. The sharp rise, however, observed in the He data below $v = 1.0$ au does not show up in the H_2 data. This difference is essentially related to the behaviour of the proton stopping power, which is, in the low-v range, much larger for H_2 than for He [40]. The theoretical stopping power ratios shown in figure 7 correspond to an *atomic* H target and have been obtained by combining the present AO and DW stopping powers for antiprotons with AO results (this work) and DW results [25] for protons. The AO and DW curves both follow the trend of the experimental curve down to $v \approx 1$ au, but neither calculation is able to explain the weak velocity dependence of the experimental data in the low-v range. Notably, both calculations (in particular, the AO calculation) yield proton stopping powers in good agreement with the H_2 data down to $v \approx 0.5$ au. So the discrepancies between theory and experiment in the stopping power ratios of figure 7 essentially reflect the corresponding discrepancies for the antiproton stopping power as exposed by figure 5.

We note that CTMC calculations have been performed also for the stopping power of negative particles in atomic hydrogen [20, 41]. The agreement with the present AO results is good.

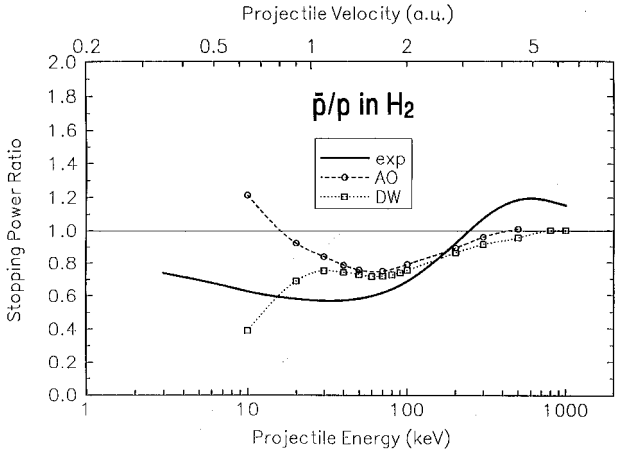

Figure 7. Ratio of antiproton to proton stopping power in H_2, plotted as a function of projectile velocity v and of projectile kinetic energy. The experimental results have been derived from the $\bar{p}$ data of [2] and from the proton data of [40] (3 to 10 keV) and the fit curve of [23] (> 10 keV). The theoretical results have been calculated for an atomic H target (AO: present work; DW: [25]).

5. Summary and conclusions

In this paper, we have performed a comprehensive analysis of the stopping power of antiprotons and negative muons in He and H_2 gas targets for projectile velocities (equivalent antiproton energies) ranging between about 0.1 and 10 au (0.25 keV and 25 MeV). Recent experimental data have been compared to stopping powers calculated from different theoretical approaches. It appears that the analysis has provided a good understanding of the basic stopping mechanisms of negative particles in gases.

When assessing the agreement between experiment and theory in detail, one has to realize two points. First, the uncertainties of the data are fairly large. Second, the target systems considered are two-electron systems whose collision dynamics is extremely complicated in general. So it is meaningless to expect agreement to within a few per cent. Yet, by combining the evidence obtained by comparing the individual model results to the data, we have been able to identify the dominating physical processes that are responsible for negative-particle stopping in different ranges of the projectile velocity.

For the He target, we have demonstrated that higher-order effects of the projectile–target interaction set in when the projectile velocity decreases towards the stopping power maximum. This onset is equally well described by the coupled-state atomic-orbital method and by the continuum distorted-wave approach. The failure of the atomic-orbital method to provide a fully satisfactory description of the data below the stopping power maximum has been shown to be related to the neglect of dynamic two-electron effects. At low velocities, these effects are apparently much stronger in negative-particle collisions than in positive-particle collisions. In the distorted-wave approach, in addition to two-electron effects, higher-order effects of the *residual* projectile–target interaction are neglected. This may explain the large deviations of the distorted-wave results from the low-velocity He data. To properly describe the adiabatic relaxation of the electronic states at low velocities, we have devised and applied a generalized adiabatic-ionization model in which collisional-broadening effects are taken into account. The sum of the electronic stopping power calculated from this model and the nuclear-stopping contribution agrees fairly well with the data below the stopping-power maximum. This shows that ionization out of the transiently formed quasidipolar collision system is the dominant stopping mechanism of negative particles at low projectile velocities.

The analysis of the stopping power data for H_2 is apparently complicated by the molecular structure of the target. The coupled-state and distorted-wave calculations for atomic hydrogen describe the experimental data well for velocities beyond the stopping power maximum, but these calculations as well as the results of the adiabatic-ionization model deviate grossly from the data at low velocities. In order to get an idea of the effect that is brought about by the molecular structure of the target, we have introduced a quasiatomic approximation for the H_2 molecule and applied the adiabatic-ionization model to the two-centre system formed by projectile and quasiatom. Improved agreement with the data is then obtained.

Acknowledgments

One of us (PDF) acknowledges financial support from Consejo Nacional de Investigaciones Científicas y Técnicas de la República Argentina and from the European Communities International Scientific Cooperation Program. The Laboratoire de Chimie Physique—Matière et Rayonnement is 'Unité de Recherche Associée au CNRS (URA 176)'. We are indebted to W Fritsch for providing the energy curves of the $\bar{p}$He system.

References

[1] Adamo A *et al* 1993 *Phys. Rev.* A **47** 4517
[2] Agnello M *et al* 1995 *Phys. Rev. Lett.* **74** 371
[3] Kottmann F 1987 *Proc. 2nd Int. Symp. on Muon and Pion Interactions with Matter (Dubna, 1987)* ed V P Dzelepov (Dubna: Joint Institute for Nuclear Research) p 268
[4] Hauser P, Kottmann F, Lüchinger Ch and Schaeren R 1993 *Muonic Atoms and Molecules* ed L A Schaller and C Petitjean (Basel: Birkhäuser) p 235
[5] Kottmann F 1994 *Proc. Int. School of Physics of Exotic Atoms (Erice, 1994)* ed C Rizzo and E Zavattini (Trieste: INFN) p 297
[6] Barkas W H, Dyer J N and Heckman H H 1963 *Phys. Rev. Lett.* **11** 26
[7] Knudsen H and Reading J F 1992 *Phys. Rep.* **212** 107
[8] Wojciechowski P *et al* 1993 *Hyperfine Interact.* **82** 127
[9] Hvelplund P, Knudsen H, Mikkelsen U, Morenzoni E, Møller S P, Uggerhøj E and Worm T 1994 *J. Phys. B: At. Mol. Opt. Phys.* **27** 925
[10] Knudsen H, Mikkelsen U, Paludan K, Kirsebom K, Møller S P, Uggerhøj E, Slevin J, Charlton M and Morenzoni E 1995 *Phys. Rev. Lett.* **74** 4627
[11] Morgan D L 1988 *Hyperfine Interact.* **44** 399
[12] Wille U and Hippler R 1986 *Phys. Rep.* **132** 129
[13] Fermi E and Teller E 1947 *Phys. Rev.* **72** 399
[14] Wightman A S 1950 *Phys. Rev.* **77** 521
[15] Dalgarno A and Griffing G W 1955 *Proc. R. Soc.* A **232** 423
[16] Allison S K 1958 *Rev. Mod. Phys.* **30** 1137
[17] Schiwietz G 1990 *Phys. Rev.* A **42** 296
[18] Schiwietz G and Grande P L 1992 *Nucl. Instrum. Methods* B **69** 10
[19] Grande P L and Schiwietz G 1993 *Phys. Rev.* A **47** 1119
[20] Grande P L and Schiwietz G 1995 *J. Phys. B: At. Mol. Opt. Phys.* **28** 425
[21] Golser R and Semrad D 1991 *Phys. Rev. Lett.* **66** 1831
[22] Kimura M 1993 *Phys. Rev.* A **47** 2393
[23] Andersen H H and Ziegler J F 1977 *The Stopping and Ranges of Ions in Matter* vol 3 (New York: Pergamon)
[24] Rösel F, Trautmann D and Baur G 1982 *Nucl. Instrum. Methods* **192** 43
[25] Fainstein P D, Ponce V H and Martinez A E 1993 *Phys. Rev.* A **47** 3055
[26] Olivera G H, Martinez A E, Rivarola R D and Fainstein P D 1994 *Phys. Rev.* A **49** 603
[27] Fainstein P D, Ponce V H and Rivarola R D 1991 *J. Phys. B: At. Mol. Opt. Phys.* **24** 3091
[28] Bates D R and Griffing G W 1953 *Proc. Phys. Soc.* A **66** 961
[29] Bates D R and Griffing G W 1954 *Proc. Phys. Soc.* A **67** 663
[30] Bates D R and Griffing G W 1955 *Proc. Phys. Soc.* A **68** 90
[31] Hasted J B 1972 *Physics of Atomic Collisions* (London: Butterworths) ch 11
[32] Wille U 1991 *Z. Phys.* D **21** S353
[33] Fritsch W 1995 private communication
[34] Kimura M and Inokuti M 1988 *Phys. Rev.* A **38** 3801
[35] Inokuti M 1989 *Nucl. Tracks Radiat. Meas.* **16** 115
[36] Schiwietz G, Skogvall B, Tanis J and Schneider D 1988 *Phys. Rev.* A **38** 5552
[37] Bohr N 1948 *Mat. Fys. Meddr. Danske Vidensk. Selsk.* **27** No 8
[38] Besenbacher F, Andersen H H, Hvelplund P and Knudsen H 1979 *Mat. Fys. Meddr. Danske Vidensk. Selsk.* **40** No 3
[39] Herzberg G 1964 *Molecular Spectra and Molecular Structure (vol I: Spectra of Diatomic Molecules)* (Princeton: Van Nostrand) ch VI, 4
[40] Golser R and Semrad D 1992 *Nucl. Instrum. Methods* B **69** 18
[41] Cohen J S 1983 *Phys. Rev.* A **27** 167